Determination of chloride threshold initiating corrosion: A new set-up taking the localized aspect of corrosion into account

Chantal Chalhoub, Raoul François, Myriam Carcasses

Determination of chloride threshold initiating corrosion: a new set-up taking the localized aspect of corrosion into account

Chantal Chalhoub*, Raoul François, Myriam Carcassés
LMDC, INSA, UPS, Université de Toulouse, France
* Corresponding author: chantal.chalhoub@insa-toulouse.fr

ABSTRACT

In spite of much research invested in the study of concrete reinforcement corrosion induced by chlorides, there is still no agreement on an accurate method for determining the chloride threshold value initiating corrosion. The objective of this work is to present a new test set-up that considers the localized character of corrosion initiated by chlorides. This approach is based on a physical separation between the anode, contaminated with chlorides, and the cathode, which is chloride free. This approach will allow to quantify the galvanic corrosion current, making it possible to determine, in a second step, the chloride threshold values for corrosion initiation. The criteria for corrosion initiation was a threshold corrosion current defined as a current that is independent of the cathode/anode surface ratio. It was then important to test the influence of the geometric surface ratio on the galvanic corrosion current. It was found that it is an important parameter that needs to be taken into account when studying corrosion in the presence of chlorides. Preliminary results of threshold values were determined based on this criterion for CEMI and for several types of steel surface conditions. The preliminary results also give an idea of the influence of chloride contents on the galvanic corrosion currents.

1.Introduction

Traditionally, concrete reinforcement corrosion induced by chlorides is initiated when the chloride content reaches a certain threshold Ccrit. After investing much time and effort in this field, researchers have still not reached agreement on an accurate and reliable method for the determination of this threshold value [1]. Corrosion initiated by chlorides is macrocell corrosion (also known as localized or non-uniform corrosion). This means that the anodic (active steel) and cathodic (passive steel) sites are distant from one another.

Two traditional electrochemical techniques are commonly used for analysing corrosion initiation: measurement of the linear polarization resistance, and measurement of the reinforcement potential, where a potential drop would indicate the start of corrosion.

The first electrochemical method, the measurement of linear polarization resistance of steel in concrete, is supposed to provide quantitative information on corrosion kinetics, unlike the potential measurements. It is based on polarizing the reinforcement in order to shift the corrosion system from its equilibrium state. The polarization resistance obtained is then converted into corrosion current density by means of the Stern-Geary equation [2,3], which was originally established for the uniform corrosion state [4]. Unfortunately, application of the Stern–Geary [2] equation to localized corrosion found in real structures is unsuitable since it is not fundamentally correct to apply the mixed potential concept established by Wagner and Traud [5] when anode and cathode are some distance apart.

Several problems in understanding polarization measurements and their application to macrocell corrosion have been reported [6,7]. In fact, the behaviour of the macrocell system has been found to depend on the polarization direction (anodic or cathodic) and magnitude. Laurens et al. [8] proved that, when a macrocell system was polarized cathodically, the polarizing current was spread over passive areas. Conversely, it was spread over active areas in the case of anodic polarization. This means that, in localized corrosion systems, the apparent linear polarization range is underestimated when this technique is employed. Additionally, Elsener et al. [9] found that the response of a macrocell system is not the same as that of a microcell system. Recently, Angst and Büchler [10] questioned the applicability of the Stern–Geary equation for quantifying the corrosion rate using linear polarization resistance

measurements in the case of macrocell systems. All the arguments mentioned above show that the linear polarization resistance measurement does not take account of the intrinsic localized aspect of corrosion in concrete reinforcement. Consequently, it is not possible to apply this method to reinforced structures in the aim of quantifying corrosion kinetics [11].

The second method employs a technique for corrosion initiation that is commonly used because of its low cost and its ease of execution. The diagnosis of corrosion initiation cannot be made with an absolute value of reinforcement potential [12,13] as presented in the ASTM standard C876-91 [14], where the absolute potential measurement is interpreted and expressed in terms of corrosion risk. A better way is to monitor potential over time in order to identify corrosion initiation [12].

Several experimental studies were realized based on this approach. Recently , a RILEM technical committee (TC) 235-CTC [15] was formed in order to realize an appropriate test method capable of giving information related to Ccrit with tolerable measurement uncertainty. However, its ultimate aim was not achieved. Concrete samples (water/binder=0.45) embedding vertical steel bars were used. The bars were chemically cleaned followed by a pre-rusting procedure in humid environment in order to create a practice-related and reproducible steel type. The introduction of chlorides was realized with a pre-drying procedure in a drying environment followed by an immersion in a 3.3% NaCl solution in order to accelerate the chloride ingress. Yet, the test duration was found much longer than expected. The open circuit potential of the rebars was monitored and the criteria of corrosion initiation was a potential drop of at least 150 mV in a period less than 24 h with a condition that the potential remains at its level or lower for a minimum period of 7 days in order to make sure that stable corrosion takes place. The measured total chloride threshold values varied from 0.6% to 1.6% /wt. binder with an average value of 1.05%.

An experimental protocol, developed by Angst et al [16], consists on taking a number of samples from real reinforcing concrete structures where corrosion has not yet initiated and expose them to controlled laboratory corrosion testing. The main advantage of this method is that it guarantees real conditions regarding factors that significantly impact Ccrit, such as the steel-concrete interface, the type and the age of the concrete and the type and surface condition of steel. The method also allows to prevent false corrosion initiation and steel bar effects. The corrosion initiation criteria was based on the method developed by RILEM technical committee TC 235 [15].

Another experimental work, developed by Pacheco and Polder [17], was also based on this RILEM Committee work. The test specimens were formed of ordinary Portland cement (PC) and ground granulated blast furnace slag (CEMIII/B) cement with a water/binder ratio equal to 0.45 for both formulations. The surface condition of the bars was as received steel with possible presence of oxidation products on some areas. The critical total chloride contents of the PC specimens ranged between 0.3 and 1 %/wt. binder with an average value of 0.56%.

V. Nygaard and Geiker [18] developed an experimental method that allows to accelerate chloride ingress decreasing the time needed to initiate corrosion. The chloride ingress was realized by a sample drying followed by their immersion in saline solution. The authors stated that there can be adverse effects of the conditioning used, mainly for the drying part (such as the non-saturated pores and/or coarsening of the pore system) which can lead to lower Ccrit. In this case, the corrosion activity of the bars was monitored by potentiostatic control. In fact, a current was applied to the steel electrodes to maintain their fixed potentials and corrosion initiation was defined as an increase of the applied current to more than 50 µA. The critical chloride found on CEMI concrete samples (Water/binder =0.45) ranged from 0.52 to 0.74 %. wt. binder. However, galvanostatic or potentiostatic control prevents repassivation which can occur under site conditions. The polarization method is then considered to be non-representative and conservative [15].

Garcia et al [19] used the same corrosion initiation criteria presented earlier and found, in case of CEMI, Ccrit values that ranged between 0.6% and 0.9% per weight of cement.

This technique, also implemented in others several studies [20–23], does not provide any quantitative information about corrosion kinetics. Moreover, the results obtained by Garcia et al. [19] indicate that it is no longer useful in cases of formulations with slag and pozzolanic additives. It was found that, for formulations with high substitution levels of slag, the potential values were very low from the beginning of the potential monitoring (between -600 and -700 mV/SCE), despite the absence of corrosion, and that no potential drop occurred with the initiation of corrosion. This implies that the detection of corrosion initiation using a potential drop could be difficult in cases where the potential is highly negative, for example in slag cements or in other binders containing sulfide [16].

It was therefore necessary to propose a new test protocol that would reproduce the localized chloride-induced corrosion found in real structures. This test method consists on the same components found in the other protocols discussed earlier (such as the steel bar surface condition, the alkaline environment, the procedure to introduce and measure the chlorides and the exposure conditions) but with the addition of another component which is the galvanic corrosion current. Hence, the test set-up described here is based on a physical separation of the anode part, contaminated with chlorides, from the cathode part, which is chloride free. In order to estimate corrosion rates and predict lifetime of reinforced concrete structures subjected to chloride-induced corrosion, the macrocell current is of main concern. This new experimental approach will allow the galvanic corrosion current to be quantified, thus making it possible to determine in a forthcoming work the chloride threshold values for corrosion initiation for all kind of binders including high slag contents. Preliminary results of threshold values were determined based on a threshold corrosion current that is considered independent of the surface ratio between cathode and anode. It was then important to test the influence of the geometric surface ratio on the galvanic corrosion current. It was confirmed that it is an important parameter that needs to be taken into account when studying corrosion in presence of chlorides.

With this test, it is also possible to study the influence of several parameters on corrosion propagation: anodic, cathodic, ohmic, geometric and environmental mechanisms. The preliminary results presented in this paper provide an idea of how chloride contents and the nature of the steel surface influence the galvanic corrosion currents.

2.Electrochemical background on the macrocell corrosion system

Corrosion initiated by chlorides is an electrochemical phenomenon involving two mechanisms, one of oxidation and the other of reduction. The anode, where the oxidation of the steel takes place, generates electrons needed for the reduction reaction of dissolved oxygen at the cathode. In the case where the anode and cathode are spatially combined, the corrosion is said to be uniform and is also known as microcell corrosion. In this case, the potential field is uniform and there is no current flowing in the concrete volume.

On the other hand, when the anode and cathode are spatially separated, the corrosion is said to be macrocell or non-uniform. This type of corrosion, also known as galvanic or localized corrosion, is encountered in reinforced concrete structures exposed to aggressive agents such as chlorides. In fact, the reinforcing steel in concrete is naturally protected against corrosion by a passivation phenomenon consisting of the fast formation of a dense oxide film on the steel surface. Nevertheless, this passive film may be locally destroyed by chloride ions, causing a local activation of the steel and leading to macrocell corrosion conditions.

In macrocell systems, anodic and cathodic potentials at equilibrium are different, which leads to a non-uniform electrochemical state of the steel with the presence of a potential gradient. Consequently, an ionic current circulates through the interstitial solution of the concrete between

anodic (active) and cathodic (passive) areas. This ionic current is influenced by the electrical resistivity of the concrete, which consequently affects the macrocell electronic current flowing through the metallic network. This makes the electrical resistivity of the concrete a possible control factor of the macrocell system.

A macrocell corrosion system can be defined as the electrical connection of two uniform corrosion systems: one active, representing the anode, and the other passive, representing the cathode, which results in their mutual polarization.

3.Experimental test protocol

The experimental set-up recreated localized corrosion by imposing a physical separation between the anode and cathode, which allowed the galvanic corrosion current to be measured. This was done by preparing two types of samples: the anode, representing the sample contaminated with chlorides, and the cathode, representing the sample without chlorides. To avoid the diffusion phase of chlorides and reduce the time needed for them to reach the steel surface, anodes were dried to constant weight then soaked in saline solutions.

This two-piece test set-up enabled the galvanic corrosion current to be quantified, thus making it possible to determine the chloride threshold values for corrosion initiation. It was also possible to test the influence of several parameters and mechanisms on corrosion propagation, such as the influence of anodic parameters and the ratio between cathodic and anodic surface areas (noted C/A ratio). The size of the anode was chosen to be small despite the fact that, in reality, the anode forms spontaneously on larger rebar surfaces. The reason behind this is to have an anode steel bar that is, as much as possible, in an active state. In real structures, the C/A ratio is very high at the beginning of the corrosion process because of the multiple layers of reinforcement bars that are still initially in the passive state. For this reason, in the present test, a high C/A ratio, of 16, was chosen. Moreover, it was important to choose a sufficiently large C/A ratio that is equal to 16 because lower C/A values may lead to corrosion currents that are difficult to measure.

3.1. Description of test specimens

3.1.1 Specimen characteristics

The cathodic samples were cylindrical (ϕ110 x 220 mm) with a cover of 5.2 cm. At the centre of each sample was a 160 mm long Fe-500 ribbed steel bar 6 mm in diameter. The anodic samples were also cylindrical (ϕ33 x 70 mm) with a steel bar of 10 mm length and 6 mm diameter embedded at the centre of each one, thus having a cover of 1.35 cm.

Two electrical wires were tin welded to each steel bar, one to the upper part and one to the lower, leaving only the lateral surface of the steel uncovered. The upper wire was used to guarantee a good electrical connection during electrochemical testing. Each wire was held in place by a hole made in the middle of the upper and lower part of the plastic mould. The rebar was thus maintained in the middle of the specimen. The lower wire was fixed to the hole of the base of the mould with a knot, which was then covered in silicone.

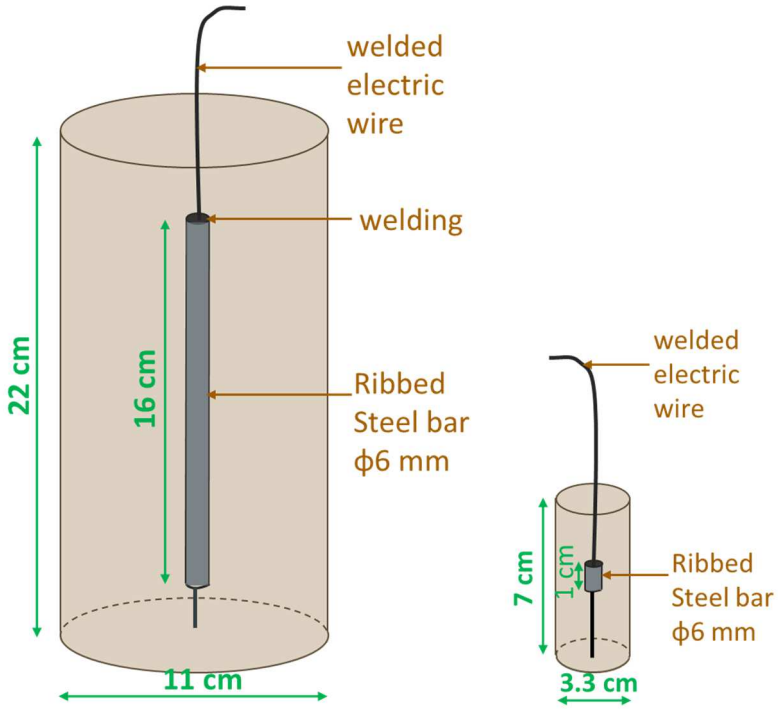

Fig. 1. Dimensions of the cathodic (left) and anodic (right) test specimens

3.1.2 Mortar composition and its characterization

The use of reinforced mortar specimens instead of reinforced concrete allowed small samples to be made without recourse to core cutting. The mortar formulation used and its characteristics are presented in Table 1 and Table 2, respectively. The water/cement ratio used was 0.55 and the sand/cement ratio was 2.75.

CEM I Mortar mixture	
Materials	Quantity (kg/m3)
Siliceous sand 0/4	1408
CEMI 52.5 R (Lafarge factory)	512
Water	281.4
Water/Cement	0.55

Table 1. Mortar formulation

Characterization tests	CEMI					
	10 days		28 days		90 days	
Compressive strength (MPa) (NF EN 196-1)	59	$\bar{X}$=56 σ=2	65	$\bar{X}$=66 σ=1	78	$\bar{X}$=75 σ=2
	54		68		75	
	56		65		74	
Water porosity (%) (AFREM)	21.5	$\bar{X}$=21.7 σ=0.20	21.3	$\bar{X}$=21.2 σ=0.34	20.86	$\bar{X}$=21.0 σ= 0.15
	21.7		21.5		21.06	
	22		20.7		21.22	
	20.15	$\bar{X}$=20.11	20.22	$\bar{X}$=19.68	17.16	$\bar{X}$=16.73

Chloride migration coefficient (10-12 m2/s) (NtBuild 492)	19.79	σ=0.24	19.48	σ=0.39	17.02	σ= 0.52
	20.38		19.33		16	
Electrical resistivity (Ω.m) (RILEM TC-154 EMC)	106	$\bar{X}$=109	114	$\bar{X}$=123	120	$\bar{X}$=128
	111	σ=3	132	σ=9	135	σ=8

Table 2. Characterization results on the mortar obtained at 10, 28 and 90 days of curing age

3.1.3 Steel bar reinforcement types

It is essential to understand the effect of the surface condition of steel on rebar corrosion. In fact, reinforcement bars are often covered with a layer of mill scale (high temperature phase formed during the cooling of iron) which may or may not be combined with a layer of corrosion related to the action of rainwater or formed during prolonged outdoor exposure on site.

The non-uniformity of mill scale could lead to the concept of weakest spot. The weakest spot could be related to the geometry of the rebar such as the presence of ribs which can induce different cooling kinetics during the industrial process. On the other hand, the weakest spot could be related to damages after manufacture for instance during the handling or during the assembly of the bars on construction site. It could also be related to size effect in casting process for instance the heterogeneity of the steel/concrete interface.

If the weakest point is induced by the rebar damages or size effect, this limitation cannot be resolved in a laboratory experimental test even if a bigger length of anode rebar was used. Knowing that, in reality, the length of the bars is approximately 6m whereas the length of the bars used as anodes, in experimental works, usually do not exceed 0.1 m.

However, if the weakest point is associated with the geometry, it is possible to resolve this issue by using different types of steel surface conditions. For instance, it is possible to use a certain treatment that eliminates the effects of formation of mill scale during the cooling of rebars by using an acid cleaning technique followed with a heating treatment that allows the formation of a new layer of corrosion products that is supposed to be more uniform than mill scale.

Four different types of steel surface were used in this study (Fig. 2):

Fig. 2. Different types of steel bars used: ARS, CS, CSPT and CSPH

• As Received Steel, “ARS”: steel without treatment presenting a non-uniform layer of mill scale, which is the case for many reinforcement bars on site.

• Cleaned Steel, “CS”: steel cleaned with a chemical cleaning procedure based on standard ISO 8407 [24], which uses an acid solution to remove the mill scale layer. The weight difference of the steel bar before and after the cleaning treatment was measured on 96 different bars and had an average value of 2.2μ mg with a coefficient of variation (CV) of 28.8%. This value could represent the weight of the mill scale layer at the steel surface.

• Cleaned Steel Pre-oxidized by high Temperature, “CSPT”: steel cleaned then oxidized with a heat treatment of 72 h at 400 ^{o}C in order to obtain a homogeneous layer of corrosion products having a composition close to that of the mill scale found in the case of ARS bars, which is made up mostly of magnetite with a little hematite. The weight difference after cleaning of the samples was measured before and after the heat treatment on 48 different steel bars. The weight difference was around 0.67

mg (CV=38.4%) and represented the weight of the layer of corrosion products formed at the surface of the steel bars during the heating treatment.

• Cleaned Steel Pre-oxidized by exposure to Humid environment "CSPH": steel cleaned then oxidized for two weeks in a humid environment (relative humidity=95%) in order to study a non-uniform oxidation layer formed in the absence of mill scale.

The steel type abbreviations explained in this section are used in the rest of the paper. The weight of the anodic steel bars was measured with a precision of 0.0001 g before the wires were welded, in order to quantify the steel weight loss before and after corrosion.

3.1.4 Preparation of mortar samples

Once prepared and mixed, the fresh mortar was poured into the corresponding moulds in two layers, each of them being vibrated for approximately 30 seconds in order to eliminate air voids. During the vibration, it was important to keep the steel in the middle of the mould by pulling the electrical wire vertically. After casting, the surface of the specimens was covered with a plastic cover to prevent the evaporation of water. The upper wire was inserted in the hole of the cover and fixed with adhesive tape. Then, the specimens were placed in a curing room where the relative humidity was approximately 95%. All the specimens were unmoulded after 24 hours and then cured for 28 days in the same wet curing room.

3.2. Processing of anodic specimens

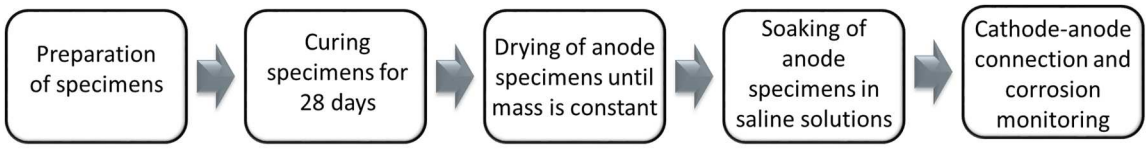

Fig. 3. Schematic representation of the specimen processing

3.2.1 Drying of anodic specimens

After the end of the wet cure, the anodic specimens were dried at a constant temperature of 45 °C and a controlled relative humidity of 25% until their mass was constant, i.e. until 2 successive weighings before and after 24 hours in the oven did not differ by more than 0.05%. The temperature was limited to 45 °C to avoid the destabilization of hydrates and cracking. The drying time necessary for the stabilization of the mass of the anodes and consequently the extraction of all the existing water in the connected pores was between 25 and 35 days (Fig. 4). The average volume of dried water was calculated with equation (Eq. 1). It corresponded to 15.7% of the apparent total volume of the mortar specimen and represented almost 75% of the water porosity of the formulation used.

$$V_{dried}\ (L) = \frac{W_{dried}}{\rho_{Water\ meas}} \qquad \textit{Eq. 1}$$

W_{dried} : Weight of the water dried from connected pores determined by the mass difference found when measuring the anodic sample before and after complete drying (g);

$\rho_{Water\ meas}$: Density of water measured experimentally at 20 °C, with a value of 995 g/L.

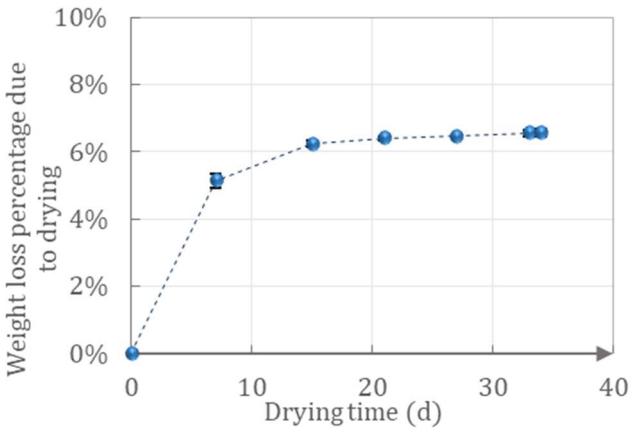

Fig. 4. Stabilization of the weight loss of anodes during their drying in the oven

During their drying period, anode specimens could be subjected to carbonation. It was then important to see if the anode specimens were carbonated during drying. For this reason, some dummy specimens having the same dimensions of the anode but without reinforcement, were dried in the same environment of the anode specimens. After more than one year of drying, phenolphthalein solution was sprayed onto the freshly cut surfaces of those samples in order to determine the carbonation depth. A solid purple coloration was observed on the entire surface indicating that there was no carbonation during the drying of anode samples.

3.2.2 Immersion of anodic specimens in saline solutions

After the end of drying, the chlorides were introduced by soaking the anodes in 1 L of sodium chloride solutions having controlled chloride contents using demineralized water. The electrical wires welded to the bars were coated with silicone to avoid chloride penetration into the samples through the wires. The samples were entirely immersed for 48 hours in saline solutions with 5 different concentrations of NaCl: 12.25, 22.75, 70, 140 and 280 g/L. Hence, a priori, known quantities of chlorides were present in the anode samples. Their quantities were also measured a posteriori, after the destruction of the specimens to check the corrosion state. On the other hand, the cathodes, which were chloride free, remained intact and could thus be reused.

5 reference samples identical to the anode samples but without steel bars were contaminated with the different saline solutions for a period of 168 hours. The weight of the samples was measured before and after soaking at different imbibition durations. After 48 hours of soaking, the weight of saline solution absorbed by the sample (W_{abs}) according to the initial weight of the sample ($W_{initial}$) had almost stabilized (Table 3). This means that a period of 48 hours of soaking is an optimal duration for the immersion of anode samples in saline solutions.

[NaCl] (g/L)	W_{abs} / $W_{initial}$ (%)						
	Imbibition duration (h)						
	0	5	24	**48**	72	96	168
280	0%	6.9%	7.6%	**7.7%**	7.7%	7.7%	7.8%
140	0%	7.0%	7.2%	**7.2%**	7.2%	7.2%	7.3%
70	0%	7.0%	7.0%	**7.0%**	7.0%	7.1%	7.2%
22.75	0%	6.6%	6.6%	**6.7%**	6.7%	6.7%	6.8%
12.25	0%	6.9%	6.9%	**6.9%**	6.9%	7.0%	7.1%

Table 3. Weight percentage of absorbed saline solution according to duration of soaking

3.3. Methods for corrosion assessment

At the end of the corrosion test, a steady state polarization test was performed on samples. This test is not presented and not used in this paper but will be exploited in a forthcoming work. Then, the chloride contents were determined for all the anode samples. All of the CS, CSPT and CSPH and some of the ARS specimens were used for the characterization of the steel/mortar interface. Most of the ARS specimens were used for visual and optical inspection and gravimetric measurements. Each of the analysis methods presented in Fig. 5 is detailed below.

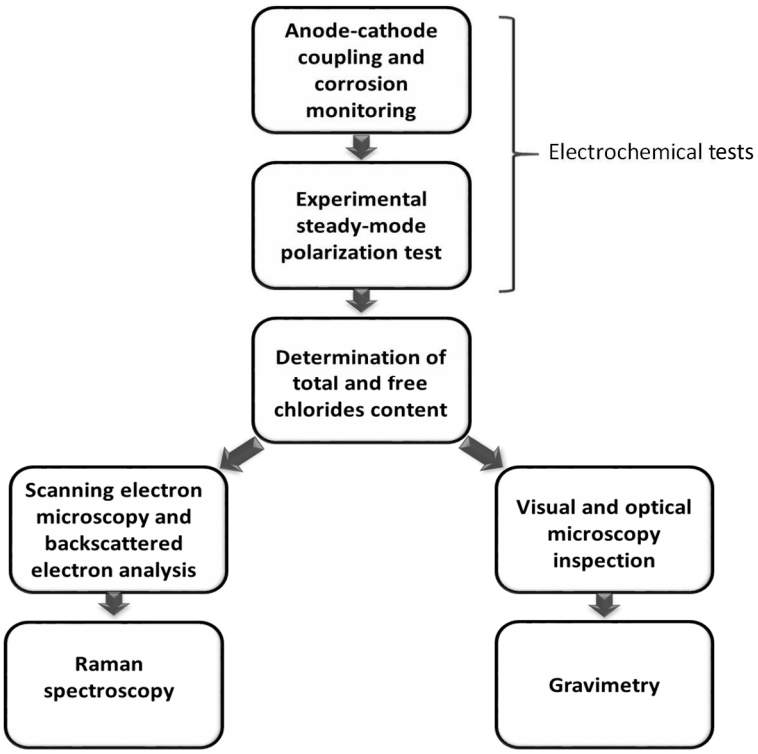

Fig. 5. Summary of the corrosion analysis methods used

3.3.1 Anode-cathode coupling and measurement of galvanic corrosion current

After two days of immersion in the saline solution, each anodic specimen was placed, with the corresponding cathode, in a sodium hydroxide solution (NaOH). The anode and cathode samples were separated by a distance of 30 cm, leaving 1 cm of the anode and 3 cm of the cathode not immerged in the alkaline solution. The pH and electrical conductivity of the sodium hydroxide solution were measured with a pH meter and a conductivity meter, respectively (Table 4). Since NaOH reacts with carbon dioxide from the air, each solution prepared for the test was renewed after 7 days in order to maintain the same concentration and thus the same pH.

Age (days)	pH	Electrical conductivity (mS/cm)
0	12.31	57.1
7	12.21	26.42
7	12.20	27.47

Table 4. pH and electrical conductivity of NaOH solution measured at different ages

The anode and cathode samples were connected by a potentiostat controlled by EC-Lab® software using the ZRA (Zero Resistance Ammeter) electrochemical technique to measure the galvanic coupling current between them (Fig. 6). The measurement of the current was maintained for 7 days in order to reach the steady state (stabilization of the measured galvanic current). All the electrochemical experiments were carried out at a constant temperature of 20 °C in a controlled room.

It is important to note that, if the anode was left alone after chloride soaking, intrinsic localized corrosion due to chlorides led to non-uniform corrosion on the anode (called inside macrocell), which was assumed to be negligible in comparison with the galvanic corrosion. Further research will be needed to assess the proportion of inside macrocell corrosion of the anode in comparison with the galvanic current measured.

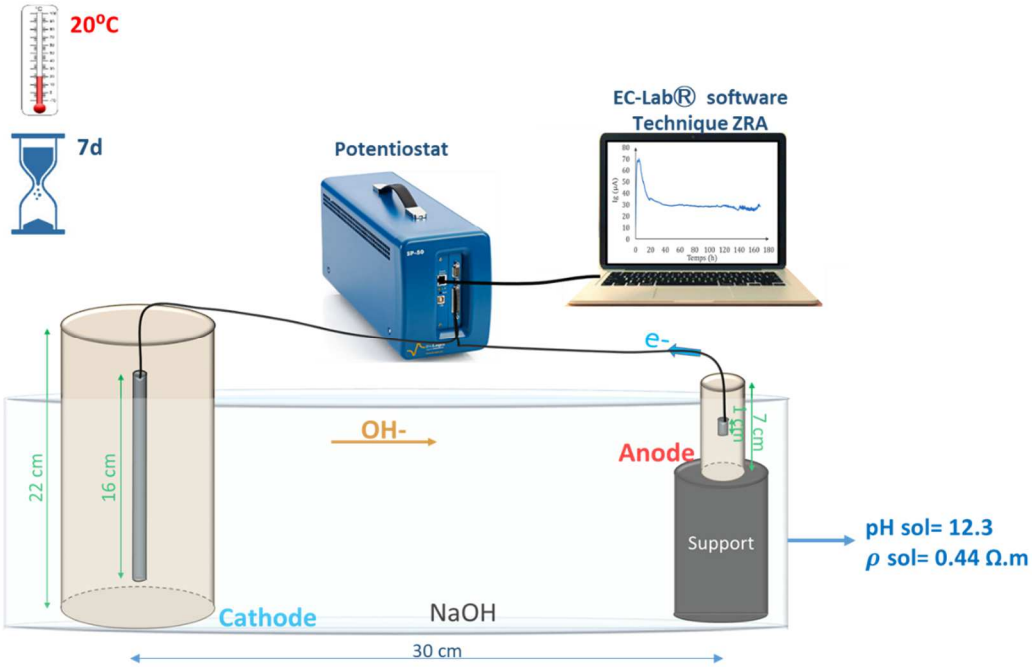

Fig. 6. Cathode-anode coupling and measurement of the galvanic current

This two-specimen system allowed the galvanic current between anodic and cathodic areas to be quantified, which has not been possible in the single-specimen systems developed in the literature [15]. This galvanic corrosion current was evaluated according to the chloride contents and the nature of the steel surface.

The potentials of the anode and cathode were measured before the two samples were connected and the potential was tracked for one hour after the samples had been disconnected at the end of the corrosion test. Generally, the potentials measured with respect to a reference electrode located on the surface of the concrete do not represent the real potential of the reinforcement. These potentials depend on the position of the reference electrode because of different phenomena such as junction potential at all interfaces, gradient of concentration in the embedding mortar, etc. In this test, the geometry of the anode specimens and cathode samples was the same and the samples were symmetrical, with a constant cover thickness regardless of the position of the reference electrode. Hence, it was possible to compare the potential measurements.

3.3.2 Determination of total and free chloride contents per mass of cement

Total and free chloride (Cl) contents were measured at the end of the corrosion test in all of the anode samples to relate the measured chloride levels to the experimental galvanic currents. The

dissolution of powders for the determination of total chlorides (free and bound) was carried out according to standard NF-EN-14629 [25] and the preparation of solutions for the free chlorides followed the procedure recommended by GranDuBé [26]. The determination of chlorides in mortar powder requires a sample weighing between 1 and 5g. Thus, mortar was taken at the level of the steel bar after splitting the sample in the middle and removing a thickness of 5 mm of mortar from either side (Fig. 7) to obtain almost 6 g of powder. Approximately 2 g was used for the quantification of total chlorides and 4 g for the free chlorides. The volumetric analysis was performed with the Ti amo software by precipitation with a silver nitrate solution.

In order to confirm whether the soaking procedure led to the estimated chloride contents in the vicinity of the rebar, these measurements were also made on 6 reinforced reference samples directly after 48 hours of soaking, without their coupling with a cathode (hence avoiding possible chloride accumulation induced by the potential gradient resulting from the corrosion test). These control specimens were soaked in 5 different saline solutions with the 5 concentrations mentioned in part 3.2.2, and in demineralized water. To make sure that this sampling method was reliable and repetitive, we also measured the free chlorides on 4 g of powder with the GranDuBé method, then the remaining chlorides, which represented the fixed chlorides, with the NF-EN-14629 standard. The results presented in Table 5 show that the sum of the free and fixed chlorides was almost equal to the level of total chlorides.

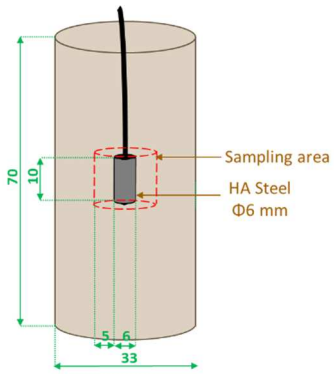

Fig. 7. Sampling area for the determination of chloride content (dimensions in mm)

	Experimental results (%/wt. cement)				calculation
	2 g of powder	4 g of powder	4 g of powder		Free Cl + Remaining fixed Cl
[NaCl] (g/L)	Total Cl (NF-EN-14629)	Free Cl (GranDuBé)	Free Cl (GranDuBé)	Remaining fixed Cl (NF-EN-14629)	
0	**0.09**	0.03	0.03	0.06	**0.09**
12.25	**0.29**	0.16	0.17	0.12	**0.29**
22.75	**0.43**	0.30	0.28	0.12	**0.41**
70	**1.03**	0.89	0.88	0.18	**1.05**
140	**2.80**	2.59	2.50	0.31	**2.81**
280	**5.03**	4.68	4.69	0.38	**5.07**

Table 5. Application of the titration procedure on 6 reference samples

Knowing that the total chlorides are the sum of free and fixed chlorides, the shift from total to free chlorides could also be theoretically achieved using adsorption isotherm equations, which are empirical relations between the concentrations of a solute on the surface of an adsorbent and the concentration of the solute in the liquid with which it is in contact. The relationship between bound and free chlorides can be described by the Freundlich isotherm for high free chloride concentrations (Fig. 8). This relation (Eq. 3) is often used to describe isotherms because it correlates well with the experimental data.

$$\text{Fixed Cl} = \alpha\ \text{Free Cl}^{\delta} \qquad \textit{Eq. 2}$$

With:

- Fixed Cl (%/wt. cement): Quantity of bound chlorides in the solid phase;
- Free Cl (%/wt. cement): Quantity of free chlorides in the pore solution;
- α and δ: Empirical coefficients.

The empirical coefficients are determined by fitting the Freundlich equation (Eq. 3) with the results obtained with the reference samples mentioned above, giving α=0.2 and δ=0.4 with a correlation coefficient of 0.98.

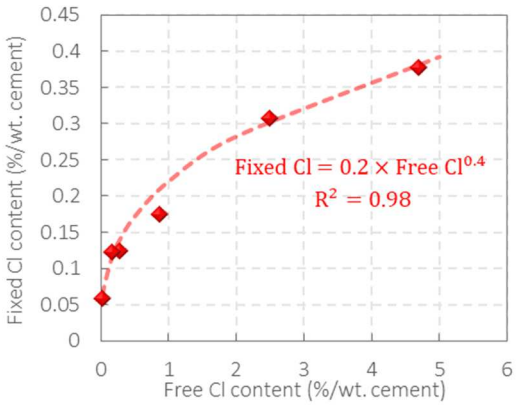

Fig. 8. Freundlich isotherm for the fixation of chlorides after 48 h in the case of the formulation presented in Table 11.

3.3.3 Visual and optical microscopy inspection

Once the anode had been split in the middle, it was simple to remove the steel. Then, the steel bar could be observed visually and with a microscope to detect the presence of corrosion products (Fig. 9-a). The steel bar was then cleaned to remove all the corrosion products at the steel surface, following the ISO 8407 standards [24]. This cleaning method consists of light mechanical cleaning treatment combined with a chemical cleaning procedure using a solution of hydrochloric acid, antimony trioxide and tin (II) chloride. The steel was then directly observed with a microscope and 4 images were taken on 4 different sides of each sample in order to cover the whole cylinder. The area of the corroded steel surface was estimated on the images using ImageJ software (Fig. 9-b), which is an open source image processing program designed for scientific multidimensional images. The error involved when moving from a 3D object to 2D images was considered negligible even though the diameter of the steel bar is small (6 mm).

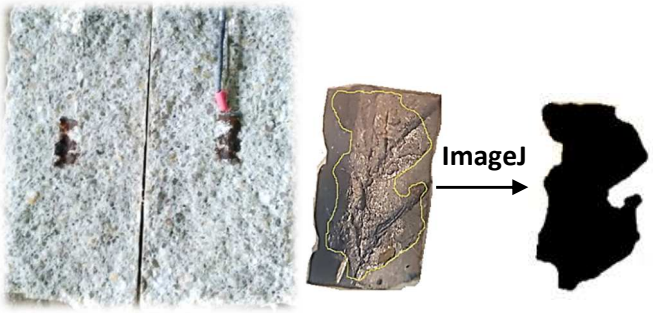

(a) (b)

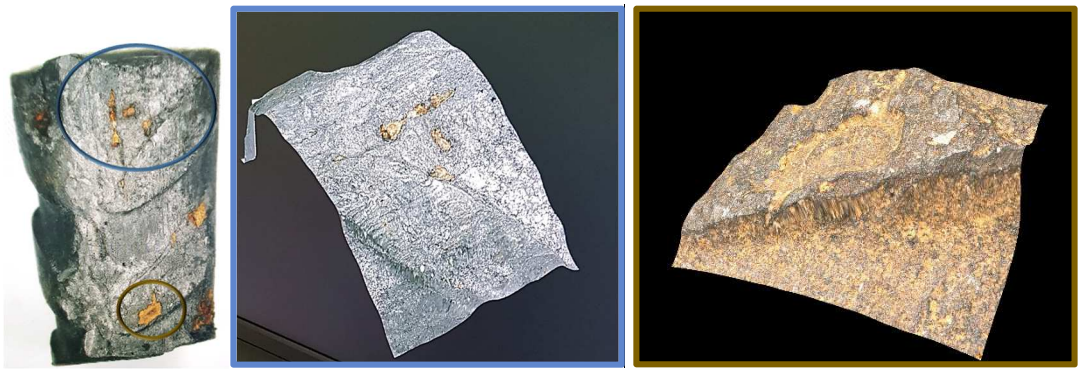

(c)

Fig. 9. (a) Splitting of the anode and visual detection of corrosion products. (b) Image processing of 1 side of a steel bar using ImageJ. (c) 3D observation with KEYENCE digital microscope of a steel bar corroded for 70 days

3.3.4 Gravimetric measurements

After the cleaning treatment and the microscopic inspection, the steel was weighed. The difference between the initial mass (weight of the steel measured before mortar casting) and the final one (weight after experiment and cleaning) gave the total mass loss of the steel. However, it was important to exclude the metal loss resulting from cleaning. This was determined using 96 different control specimens of steel bar. The average mass loss of the control specimens was around 2.23 mg (Coefficient of Variation CV=28.8%), which reflected the mass lost by test specimens in the cleaning procedure. Gravimetric measurements were only performed on ARS steel, since all of the CS, CSPT and CSPH and some of the ARS specimens were used for the characterization of the steel/mortar interface. Hence, there was no need to correct the mass loss to take account of that associated with the pre-cleaning and pre-corrosion treatment. The steel mass loss resulting from the polarization test, when realized, was also calculated using Faraday's law and subtracted from the total weight loss.

4. Results and discussion

4.1. Experimental macrocell corrosion current

4.1.1 Determination of the average corrosion current

As mentioned previously, the localized aspect of corrosion initiated by chlorides was even observed on the small anode (Fig. 9). This means that the anode was partially active and therefore behaved as a localized corrosion system. Consequently, it was necessary to separate the three types of current presented in Fig. 10, where I_g is the measured corrosion current exchanged between anode and cathode, I_a is the corrosion current exchanged between active and passive zones of the anode, and I_{micro} is the microcell corrosion current at anodic sites of the anode which was considered negligible because of the polarization of the anode during the corrosion test [11].

In a first approach, I_a was neglected because the passive area in the anode, also called the internal cathodic area, was much smaller than that of the external cathodic area, i.e. the passive area at the cathode. Further developments will be done to characterize this internal current I_a .

In the anode-cathode coupling tests, the galvanic corrosion current I_g was measured for 7 days. Fig. 11 shows the tracking of the measured corrosion current over time. Two main values of corrosion currents were considered: the instantaneous current at 7 days and the average current $I_{g\ avg}$ calculated from the integral of the current signal over a duration of 7 days. However, since the average current is more representative of the corrosion process, this value is used in the rest of this paper.

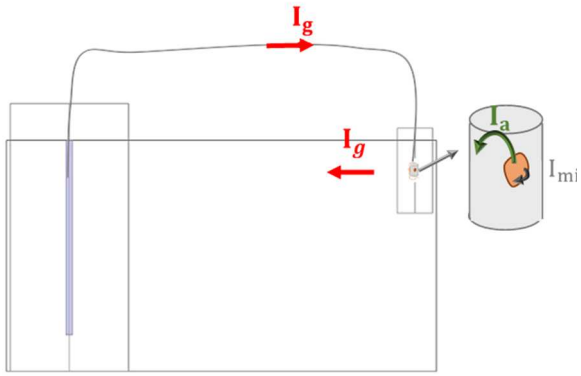

Fig. 10. Simplified schematic illustration of anode-cathode coupling showing the different types of currents

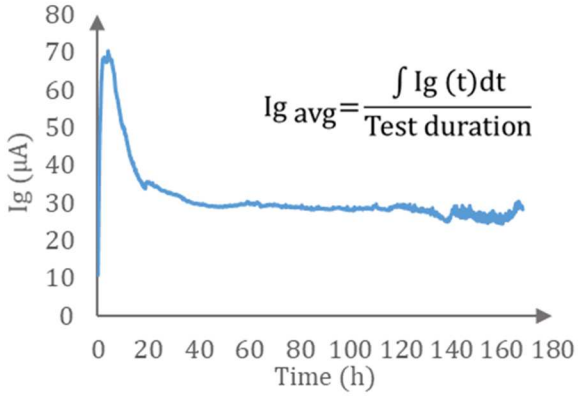

Fig. 11. Monitoring of a galvanic current measured between the anode and cathode samples

4.1.2. Influence of chloride content and steel surface condition on galvanic corrosion current

Fig. 12 presents the average corrosion currents, $I_{g\ avg}$, measured when connecting the anode and cathode according to the free chloride levels expressed in %/weight of cement and calculated from the measured total chloride contents using the isotherm presented in Fig. 8. The results are presented for the 4 types of steel described in section 3.1.3.

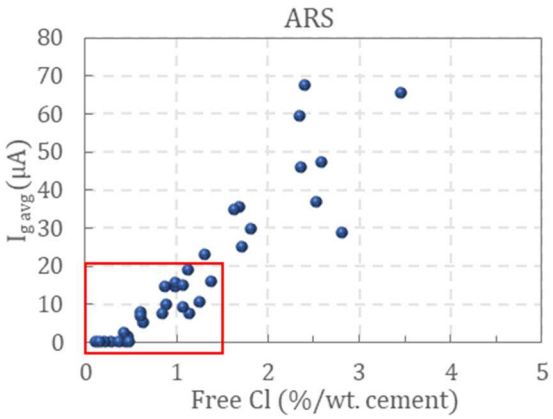

(a1)

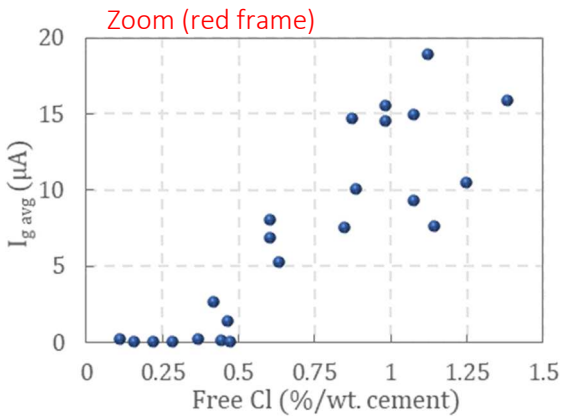

(a2)

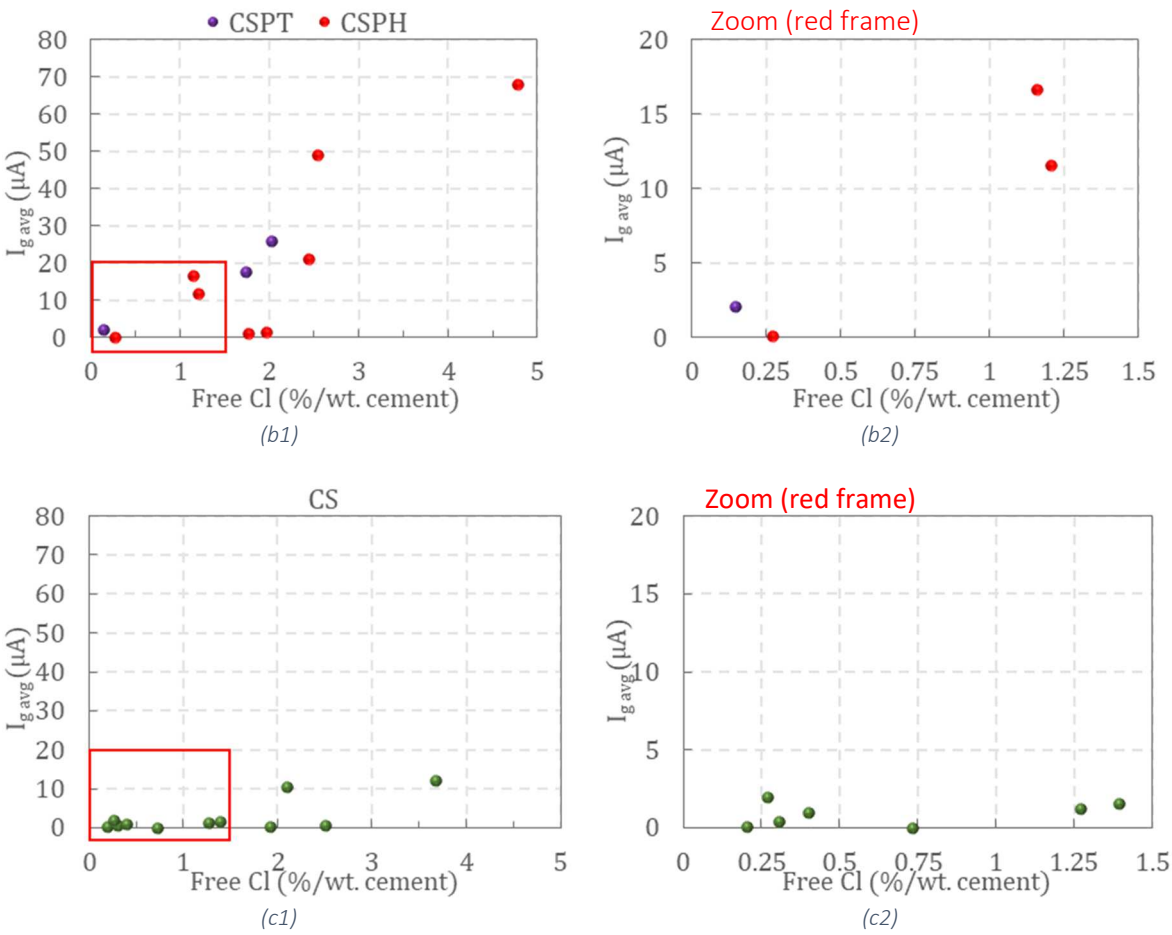

Fig. 12. Average corrosion currents according to free chloride contents (a1-2) As Received Steel; (b1-2) Cleaned Steel Pre-oxidized by high Temperature and Cleaned Steel Pre-oxidized in a Humid environment and (c1-2) Cleaned Steel

An increase of the corrosion current with the chloride level was observed for the case of as received steel, cleaned steel pre-oxidized in a humid environment, and cleaned steel pre-oxidized with high temperature. The similarity in the composition of the mill scale layer found on the as received steel and the layer of corrosion products formed on cleaned pre-oxidized steel could explain the resemblance of behaviour between these 3 types of steel. The non-uniformity of these layers may justify the presence of some scatter in the results obtained. Ghods and al. [27] found that the presence of micro cracks in the mill scale layer could lead to cavernous corrosion, which could partially explain the dispersion of the chloride threshold values for steel bars with presence of mill scale.

In contrast, the corrosion currents obtained for cleaned steel were weak compared to the results obtained with the other 3 types of steel. Yet, only for chloride levels higher than 2%, $I_{g\ avg}$ became significant and above 10 µA (samples CS9 and CS11). Nevertheless, Fig. 13 shows that the currents measured in the case of high chloride contents were negligible during the first few days or hours and then increased sharply. This could be attributed to a time being necessary for chlorides to diffuse through the passivation layer formed on the cleaned steel. It should be noted that the average current for those 2 test pieces was also calculated by dividing the current signal surface by the total test duration.

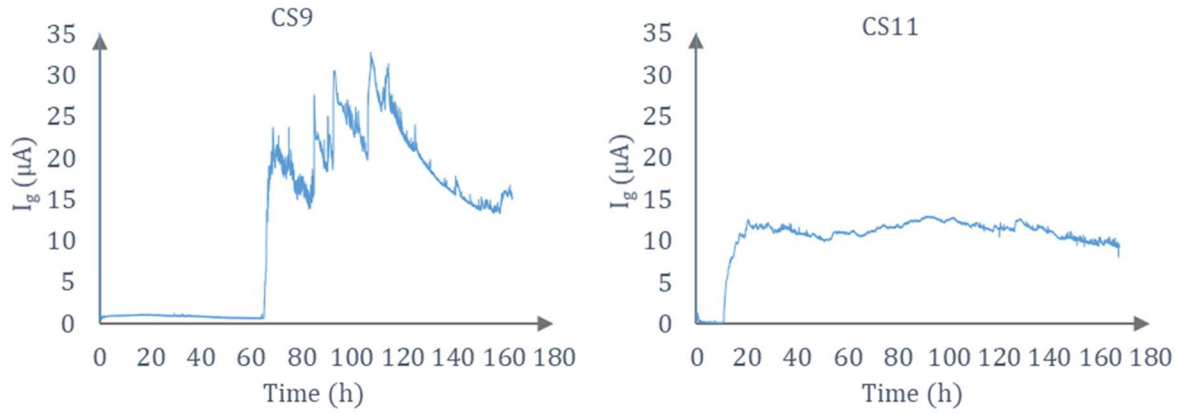

Fig. 13. Corrosion current measured in the case of cleaned steel for samples CS9 and CS11

The results obtained on the different steel surface samples allowed to make the assumption that the oxides formed on steel in the absence of mill scale (case of cleaned steel) are less porous to chloride ingress than those formed in the presence of mill scale (case of as received steel) and those formed on cleaned pre-oxidized steel.

This result is consistent with the work of E. Mahallati et al. [28] who studied the impact of the presence of mill scale on steel bars using cyclic polarization experiments. It was found that the formation, development and maintenance of the passive layer was determined by the accessibility of the metal cations to combine with oxygen and hydroxide ions. Hence, the mill scale layer could create an obstacle disrupting the formation of the passive layer. Horne et al. [29] also showed that the amount of portlandite near the reinforcement was almost 30% higher in the case of polished steel than in the case of steel with a mill scale layer. This phenomenon could have the effect of enhancing the buffering capacity of concrete at the steel-concrete interface.

A similarity is observed between the results obtained in case of ARS, which has a non-uniform surface condition, and the CSPT, which has a more uniform surface condition. This would indicate that the presence of a weakest point is not only related to the presence of ribs.

4.2. Nature of corrosion products

4.2.1 SEM observation and BSE results

A Scanning Electron Microscope (SEM) JEOL JSM 6380 operating in Backscattered Electron (BSE) mode was used to study the steel-mortar interface. A Bruker Energy Dispersive Spectrum analyzer (EDS) was used to quantify Iron (Fe in blue), Oxygen (O in red) and Chloride (Cl in green) in the observation zones along an analytical line. Fig. 14 and Fig. 15 show examples of SEM images at the steel-mortar interface for CSPH and CS anode samples, respectively. The analysis is then displayed as a graph in which the horizontal axis represents the distance from the starting point of the analytical line and the vertical axis characterizes the normalized mass percentages reflecting the Fe, O and Cl content. The thickness of the steel-mortar interface layer was also measured and the maximum thickness of the non-uniform layer was recorded for each steel type (Table 6).

The elementary composition analysis of the interface in ARS, CSPT and CSPH samples revealed the presence of chlorides in the corrosion products. Furthermore, the Cl-containing corrosion deposits were circular and located at the steel/oxide interface. This means that the chloride ions penetrated through the oxide film formed on the surface of the bars to produce a chemical compound composed of Cl, Fe and O. On the other hand, in CS samples, the thickness of the layer formed on the surface of the steel was less than 50 nm. Therefore, it was not possible to quantify the elements formed at the interface even with magnifation higher than 500x.

Steel type	ARS	CSPT	CSPH	CS
Maximum thickness of the steel-mortar interface layer	100 µm	90 µm	300 µm	<50 nm

Table 6. Maximum thickness of the steel-mortar interface layer measured on anode samples

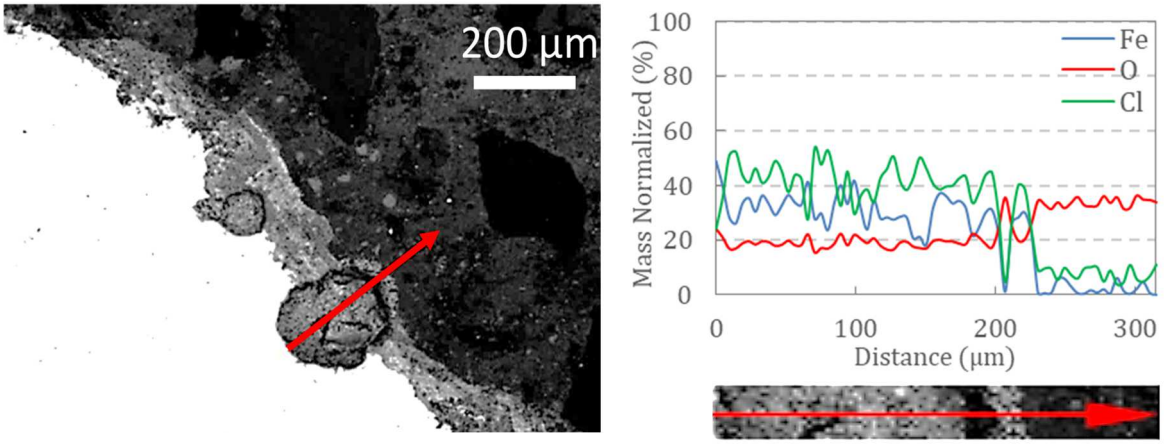

Fig. 14. Example of SEM observation and BSE analysis on a CSPH anode sample (magnifications: 110x)

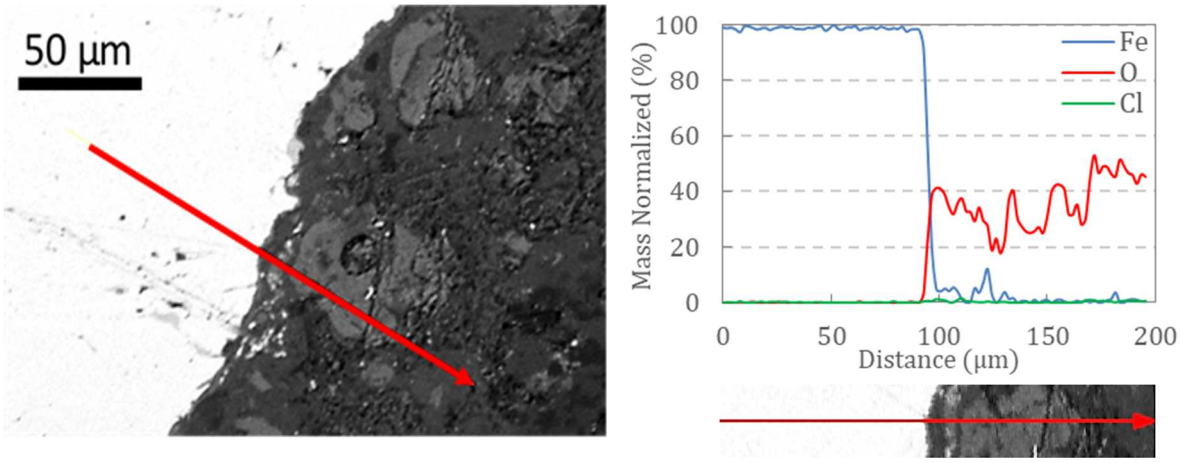

Fig. 15. Example of SEM observation and EDS analysis on a CS anode sample (magnifications: 500x)

4.2.2 Raman results

The corrosion products present at the steel/mortar interface were identified by Raman micro-spectroscopy with a Horiba spectrometer at the CEA lab at Saclay, France. The microanalyses in this study were performed with the 100x objective using the green visible radiation wavelength of 532 nm. Over the entire optical path and the detection system, the spectral resolution was about 2 cm^{-1}. Spectra were calibrated by means of a silicon crystal. The excitation laser power was filtered at 1% (acquisition time: 300s) then 10% (acquisition time: 20s) in order to avoid potential thermal transformation of sensitive iron oxides and (oxy)hydroxide [30,31]. Finally, the spectra were acquired and processed using the LabSpec software and the phases were identified by comparison with spectra existing in the literature [30,32–34] . Raman analysis was not possible in the case of CS samples because of the very thin layer of oxides. Fig. 16 summarizes the corrosion products that were found in the Raman analysis. In this figure, it can be seen that some Cl-containing corrosion products (akaganeite and iron hydroxychloride β-$Fe_2(OH)_3Cl$) were found at the steel/mortar interface on the steel side, which could explain the presence of the circular shapes containing Cl that were observed and analysed with the

SEM. The hematite and magnetite may have been corrosion products resulting from the pre-corrosion process carried out before casting.

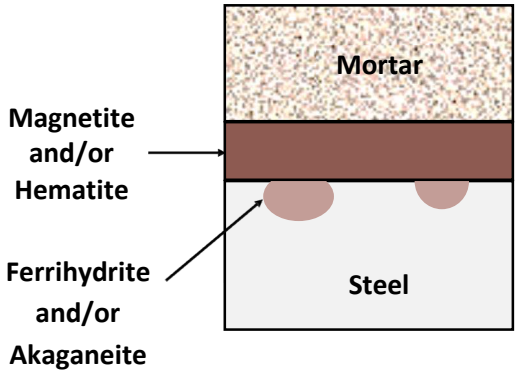

Fig. 16. Summary of the corrosion products found on CSPT and CSPH samples

4.3. Gravimetric and surface measurements

The corrosion current, $I_{Faraday}$, could be calculated theoretically from the measured loss of steel mass, using Faraday's law (Fig. 17). The mass loss of test specimens from the cleaning procedure and the steel mass loss resulting from the polarization test, when realized, were subtracted from the total weight loss. Looking at Fig. 17 we can see that the calculated currents deduced from the mass loss were slightly higher than the average galvanic currents, $I_{g\ avg}$, measured in the experiment between anode and cathode.

This mass gap can be explained by our inability to measure the internal macrocell corrosion current I_a of the anode. Despite the scatter between the two values, the measured and calculated currents showed the same trend and were relatively close, which means that I_a was relatively negligible. An increase was also observed in the active steel surface measured after 7 days of corrosion with the free Cl levels (Fig. 18).

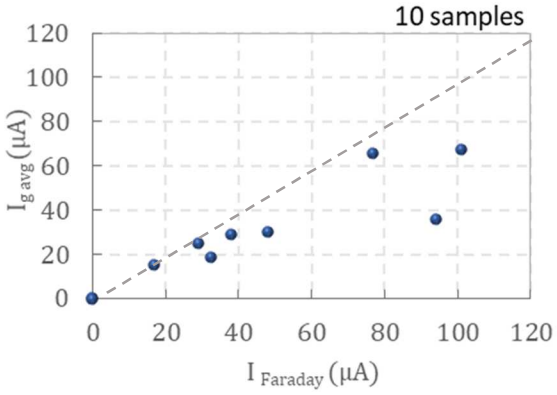

Fig. 17. Measured corrosion currents versus calculated currents with Faraday's law

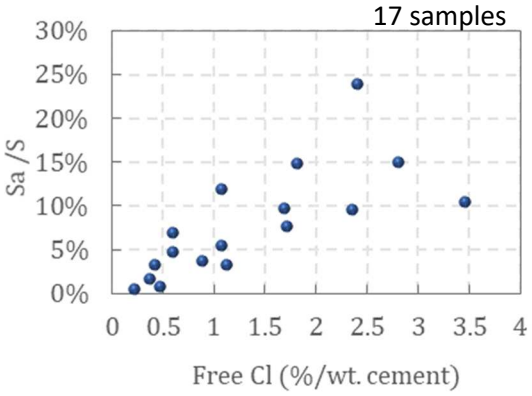

Fig. 18. Measured corroded surface area percentages according to free chloride contents

The experimental protocol presented in this work is based on the quantification of galvanic corrosion current for a C/A ratio sufficiently large that is equal to 16. This method allows to determine the chloride threshold values based on a threshold corrosion current that is independent of the area of passive steel. This current is defined as a current that does not change when the C/A ratio is higher than

16. In other words, the chloride threshold value was associated with a corrosion state that is the same whether this ratio is 16 or higher.

Knowing that the corrosion current can be influenced by the cathode/anode surface ratio, it was crucial to study the effect of this geometric parameter. In the next section, the influence of this ratio is studied and the threshold current is fixed which allows to determine the chloride threshold values of the results presented earlier (part 4).

5.Cathode/anode ratio ''C/A''

The C/A ratio is generally defined as the fraction representing the surface area of passive steel divided by that of active steel. On real structures, the formation of new anodic sites linked to chloride ingress will lead to a decrease of the C/A ratio, which is initially very high. It is thus very important to characterize the relationship between the geometric C/A ratio and the corrosion current I_g .

Several authors have studied the impact of this factor on the galvanic corrosion current. Warkus and Raupach [35] studied experimentally and numerically the influence of the C/A ratio by changing the amount of passive reinforcement in chloride-free part of reinforced structures. They found that increasing the cathodic area leads to an increase in macrocell current.

Considering that in the initiation stage of corrosion C/A ratios are extremely high, it was crucial to determine, in this work, the galvanic corrosion current, in case of very large cathodic area. It is important to recall that all the corrosion measurements made up to now were linked to a predefined geometric factor, the C/A apparent ratio, which was equal to 16. To reach very high C/A ratios, a concrete wall was used to represent the cathodic part. The dimensions of the wall are presented in Fig. 19 and its formulation is given in Table 7. The wall was a concrete parallelepiped of 75x20x100 cm containing 18 embedded steel bars of 12 mm diameter: 10 horizontal bars each having a length of 70 cm and 8 vertical bars having a length of 102 cm with 5 cm emerging from the concrete. The network of frames was completely electrically disconnected but could be electrically connected from the outside. The anode was placed in a PVC pipe containing a sodium hydroxide solution that was connected to the wall allowing the ionic current to circulate. Smaller C/A ratios were also tested. In fact, each anode was connected to 3 cylindrical cathodes (ϕ11x22cm3) with three different lengths of steel (1, 5 and 16 cm) embedded in them so as to test C/A ratios of 1, 5 and 16 respectively.

Then, the anode was electrically connected to the steel bar(s) of the wall, connecting a different number of bars each time, with different lengths presenting surface area ratios from 200 to 2950. Ten different tests were carried out using 10 different anodes that were geometrically identical but had been soaked in different concentrations of sodium chloride. Current measurements were made using an Agilent multimeter and the values of the currents were recorded after they had stabilized to a steady-state condition.

Cement	Type	CEM I 52.5 N CE CP2 NF
Sand	Type	0/4R ALL SIL CE
Gravel	Type	4/10 SR ALL SIL CE
Water/Cement		0.55
Sand/Cement		2

Table 7. Formulation of the concrete wall.

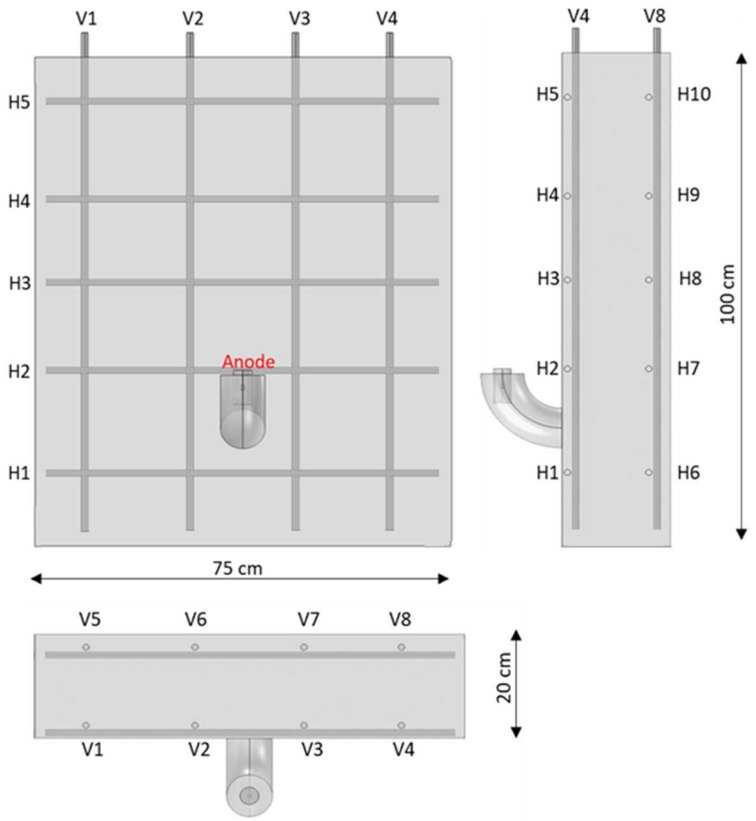

Fig. 19. Description of the concrete wall

It must be noted that the C/A ratios are presented, in this work, in terms of apparent ratios. The effective C/A ratios are based on the real anodic areas measured after splitting the samples presenting even higher ratios. Fig. 20 presents the currents measured for different C/A ratios for different free Cl levels. The free chloride levels of the samples tested are shown in the legend of the graph and are expressed in %/weight of cement. The results shown in Fig. 20 indicate that, for the same active surface area, an increase of the passive area led to an increase of the corrosion kinetics. This allows to conclude that an increase in the C/A ratio leads to an increase in the corrosion current, which is in agreement with the localized corrosion concepts mentioned above.

In fact, for a given active surface area mobilized for the anodic reaction, the intensity of the corrosion current is a function of the passive surface area mobilized for the cathodic reaction. This means that the larger the passive area is, the stronger is the corrosion anodic current [11]. Moreover, the experimental results show that the current growth rate decreases with increasing cathodic surface area, which could mean that the current will reach its maximum value and stabilize for a certain C/A ratio. Thus, it can be reciprocally concluded that the corrosion currents are high at the beginning (when the C/A ratio is high) and fall continuously when the anodic surface increases (when the C/A ratio decreases). The maximum corrosion current and the threshold stabilization ratio are associated with the chloride levels. For Cl^- levels lower than 1%, the C/A ratio does not have much influence on corrosion currents. The maximum corrosion current is also a function of the electrical resistivity of the wall. This parameter will be studied in a further step of the research.

Looking at the results obtained, we can assume that for “low” C/A ratios, corrosion is cathodically controlled. This means that corrosion current depends on dioxygen availability which is, in our case, a function of the size of cathode. On the other hand, for “high” C/A ratios, corrosion current is limited by the steel consumption, which is a function of the chloride content. An ohmic control of

corrosion is also present in this case because, when the C/A ratio increases, the cathode becomes more distant from the anode.

With this experiment, given the small size of anode and the large cathodic area, it was possible to test very high apparent C/A ratios compared to the ones studied by other authors. It was also possible to experimentally test at least 14 different C/A ratios for each anode specimen. This means that, this set-up makes it possible to determine galvanic currents for different C/A and different chloride contents.

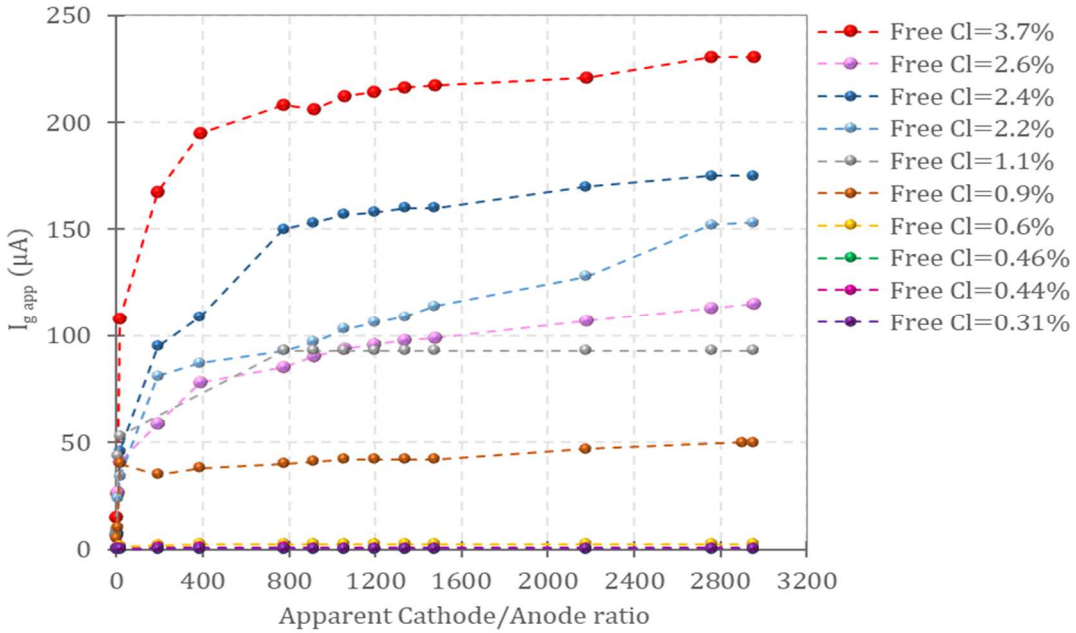

Fig. 20. Results of the experimental C/A ratio test

The effective C/A ratios were also estimated and reached very high values (almost 200000). Yet, the influence of the effective ratio on corrosion current was found the same to that obtained when dealing with the apparent ratios.

In the next part, the results obtained with both apparent C/A ratios 16 and 2950 will be presented according to the different free chloride contents. This will allow to determine the threshold galvanic current which will be the criteria for the determination of the chloride threshold value in case of a formulation formed with an ordinary Portland cement.

6.Chloride threshold values based on a chloride threshold current

Fig. 21 presents the corrosion currents exchanged between anode and cathode for different free chloride contents for the apparent C/A ratios of 16 and 2950 in case of ARS specimens.

The concept of initiation of corrosion is set according to a limit current. This implies that the initiation criteria is related to a certain limiting galvanic current that is independent of the area of passive steel. This threshold current must then be independent of the C/A ratio.

The limiting current was found equal to 3 µA. For galvanic currents lower than 3 µA, all the obtained currents are almost the same independently from the C/A ratio. On the other hand, for galvanic currents higher than 3 µA, the galvanic currents obtained with a ratio of 2950 are 3 times bigger than the ones obtained with a C/A ratio equal to 16.

Consequently, the total and free chloride threshold values for CEMI in the case of ARS, CSPT and CSPH specimens are respectively 0.6 and 0.5 %/wt. cement. However, in the case of cleaned steel, the free Cl content is 1.9%/wt. cement corresponding to a total chloride content of 2%/wt. cement.

Indeed, in Fig. 12, the galvanic corrosion current was a linear function of chloride content, with a slope change of around 0.5% of free chlorides by weight of cement in case of ARS, CSPT and CSPH specimens and 1.9%/wt. cement in case of CS specimens. The chlorides threshold values are in agreement with the discussion made earlier about the influence of the steel type condition on corrosion (part 4).

Using this approach, it would be possible to compare different types of binders, which would constitute a further step in the research.

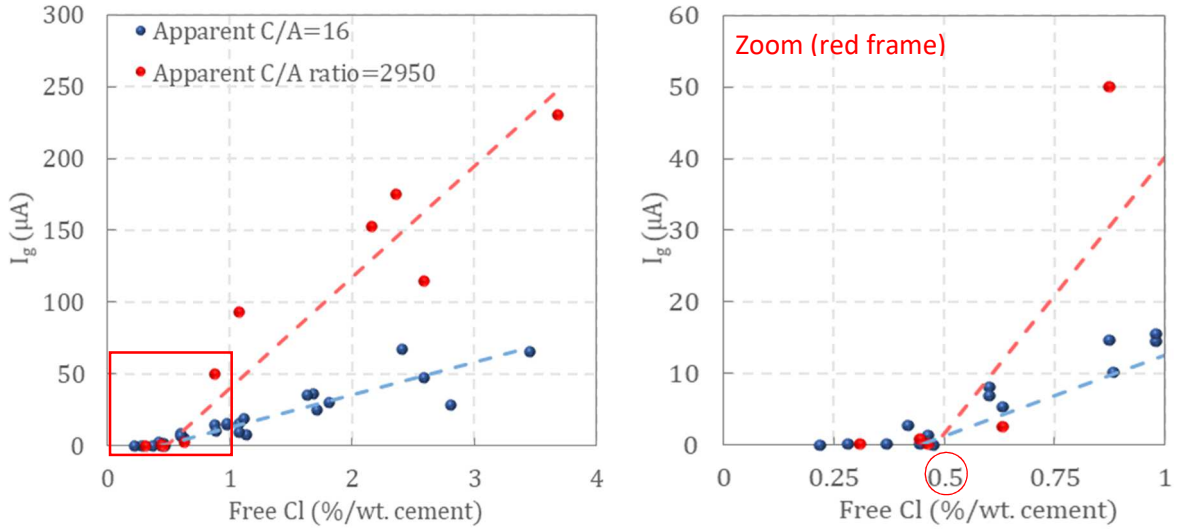

Fig. 21. Ig measured for different free chloride contents for apparent C/A ratios of 16 and 2950.

7.Conclusion

This paper has presented a new test set-up established on the localized aspect of chloride-induced corrosion in reinforced concrete structures. This two-piece system first allows the galvanic corrosion current between anodic (with chlorides) and cathodic (without chlorides) zones to be measured, which was impossible to do in tests performed on single bar specimens.

The first results presented in this paper are limited to CEM I samples. These preliminary results highlight the influence of chloride content and steel surface on the corrosion rate. It was deduced that an increase in chloride levels led to an increase in the number of "corroded sites", leading to an increase in the galvanic currents measured. The role of mill scale on corrosion kinetics was also highlighted when comparing results obtained with 4 different steel types. The similarity of behaviour between as received steel, ARS, and cleaned pre-oxidized steel, CSP, may be attributed to the resemblance in the composition of the mill scale layer found on the ARS and the layer of corrosion products formed on CSP. The non-uniformity of these layers may justify the presence of some irregular current densities obtained. The corrosion kinetics obtained in the absence of mill scale (cleaned steel specimens) were relatively weak. This phenomenon may be attributable to a less porous passive film making it harder for the chloride ions to diffuse through.

With this test, it is possible to determine the chloride threshold values initiating corrosion and also the corrosion current during the propagation stage. The criteria for corrosion initiation was set as a limiting galvanic current called threshold corrosion current. This current is defined as a current that

is independent of the cathode/anode surface ratio and was found equal to 3 µA. This indicates that the corrosion initiation must be linked to a threshold current that is not affected by surface ratio between cathode and anode. The total and free chloride threshold values for CEMI in case of ARS, CSPT and CSPH specimens are respectively 0.6 and 0.5 %/wt. cement. However, in case of cleaned steel, the free Cl content is 1.9%/wt. cement corresponding to a total chloride content of 2%/wt. cement.

Furthermore, it was confirmed that an increase in the C/A ratio led to an increase in the galvanic current, which is in agreement with the fundamental galvanic coupling concepts. The experimental results also showed that the current growth rate decreased with increasing cathodic surface area, which could mean that the current would reach its maximum value and stabilize for a given C/A ratio.

With this method, it is also possible to compare different types of binders which will be the next step of the study.

Acknowledgements

This work was supported by the ANR MODEVIE project, grant ANR-14-CE22-0018 of the French Agence Nationale de la Recherche and by the French National Federation of Public Works (FNTP).

References

[1] U. Angst, B. Elsener, C. K. Larsen and Ø. Vennesland, *Critical chloride content in reinforced concrete — A review*, Cement and Concrete Research, 39 (2009), pp. 1122–1138.

[2] M. Stern and A.L. Geary, *Electrochemical Polarization I. A Theoretical Analysis of the Shape of Polarization Curves*, Vol. 104, 1957.

[3] C. Andrade, C. Alonso, J. Gulikers, R. Polder, R. Cigna, Ø. Vennesland et al., *Test Methods for On-Site Corrosion Rate Measurement of Steel Reinforcement in Concrete by Means of the Polarization Resistance Method*, Vol. 37, 2004.

[4] A. Clément, S. Laurens, G. Arliguie and F. Deby, *Numerical Study of the Linear Polarisation Resistance Technique Applied to Reinforced Concrete for Corrosion Assessment*, Vol. 16, 2012.

[5] C. Wagner and W. Traud, *Über die Deutung von Korrosionsvorgängen durch Überlagerung von elektrochemischen Teilvorgängen und über die Potentialbildung an Mischelektroden*, Zeitschrift für Elektrochemie und angewandte physikalische Chemie 44 (1938), pp. 391–402.

[6] A. Sagues and S. C. Kranc, *On The Determination of Polarization Diagrams of Reinforcing Steel in Concrete*, Vol. 48, 1992.

[7] J. Gulikers, *Numerical Simulation of Corrosion Rate Determination by Linear Polarization*, 2015.

[8] S. Laurens, P. Hénocq, N. Rouleau, F. Deby, E. Samson, J. Marchand et al., *Steady-state polarization response of chloride-induced macrocell corrosion systems in steel reinforced concrete — numerical and experimental investigations*, Cement and Concrete Research 79 (2016), pp. 272–290.

[9] B. Elsener, *Macrocell Corrosion of Steel in Concrete - Implications for Corrosion Monitoring*, Vol. 24, 2002.

[10] U. Angst and M. Büchler, *On the Applicability of the Stern–Geary Relationship to Determine Instantaneous Corrosion Rates in Macro-Cell Corrosion*, Vol. 66, 2014.

[11] R. Francois, S. Laurens and F. Deby, *Corrosion and Its Consequences for Reinforced Concrete Structures*, Elsevier, 2018.

[12] B. Elsener, C. Andrade, J. Gulikers, R. Polder and M. Raupach, *Half-Cell Potential Measurements – Potential Mapping on Reinforced Concrete Structures*, Vol. 36, 2003.

[13] R. Francois, G. Arliguie and D. Bardy, *Electrode Potential Measurements of Concrete Reinforcement for Corrosion Evaluation*, Vol. 24, 1994.

[14] G01 Committee, *Test Method for Corrosion Potentials of Uncoated Reinforcing Steel in Concrete*, ASTM International, .
[15] L. Tang, J.M. Frederiksen, U. Angst, R. Polder, M. Cruz Alonso, B. Elsener et al., *Experiences from RILEM TC 235-CTC in Recommending a Test Method for Chloride Threshold Values in Concrete*, Vol. 3, 2018.
[16] U. Angst, C. Boschmann, M. Wagner and B. Elsener, *Experimental Protocol to Determine the Chloride Threshold Value for Corrosion in Samples Taken from Reinforced Concrete Structures*, 2017.
[17] J. Pacheco and R. Polder, *Critical Chloride Concentrations in Reinforced Concrete Specimens with Ordinary Portland and Blast Furnace Slag Cement*, Vol. 61, 2016.
[18] P. V. Nygaard and M. Geiker, *A Method for Measuring the Chloride Threshold Level Required to Initiate Reinforcement Corrosion in Concrete*, Vol. 38, 2005.
[19] V. Garcia, R. Francois, M. Carcasses and P. Gegout, *Potential Measurement to Determine the Chloride Threshold Concentration That Initiates Corrosion of Reinforcing Steel Bar in Slag Concretes*, Vol. 47, 2014.
[20] P. Sandberg, *Chloride initiated reinforcement corrosion in marine concrete*, Division of Building Materials, LTH, Lund University, 1998.
[21] U. Angst, B. Elsener, C. Larsen and Ø. Vennesland, *Chloride Induced Reinforcement Corrosion: Electrochemical Monitoring of Initiation Stage and Chloride Threshold Values*, Vol. 53, 2011.
[22] N. R. Jarrah, O. Al-Amoudi, M. Maslehuddin, O. A. Ashiru and A. Ibrahim Al-Mana, *Electrochemical Behaviour of Steel in Plain and Blended Cement Concretes in Sulphate and/or Chloride Environments*, Vol. 9, 1995.
[23] V. Bouteiller, C. Cremona, V. Baroghel-Bouny and A. Maloula, *Corrosion Initiation of Reinforced Concretes Based on Portland or GGBS Cements: Chloride Contents and Electrochemical Characterizations versus Time*, Vol. 42, 2012.
[24] *ISO 8407:2009(en), Corrosion of metals and alloys — Removal of corrosion products from corrosion test specimens*.
[25] *NF EN 14629 - Produits et systèmes pour la protection et la réparation des structures en béton - Méthodes d'essais - Mesurage du taux de chlorure d'un béton durci*. 2007.
[26] H. Hornain, *GranDuBé: grandeurs associées à la durabilité des bétons*, Presses des Ponts, 2007.
[27] P. Ghods, O. Isgor, G. A. McRae, J. Li and G.P. Gu, *Microscopic investigation of mill scale and its proposed effect on the variability of chloride-induced depassivation of carbon steel rebar*, Corr. Sci. 53 (2011), pp. 946–954.
[28] E. Mahallati and M. Saremi, *An Assessment on the Mill Scale Effects on the Electrochemical Characteristics of Steel Bars in Concrete under DC-Polarization*, Vol. 36, 2006.
[29] A. T. Horne, I. G. Richardson and R. M. D. Brydson, *Quantitative Analysis of the Microstructure of Interfaces in Steel Reinforced Concrete*, Vol. 37, 2007.
[30] D. Neff, S. Réguer, L. Bellot-Gurlet, P. Dillmann and R. Bertholon, *Structural Characterisation of Corrosion Products on Archaeological Iron: An Integrated Analytical Approach to Establish Corrosion Forms*, Vol. 35, 2004.
[31] D. L. a. de Faria, S. Venáncio Silva and M. T. de Oliveira, *Raman Microspectroscopy of Some Iron Oxides and Oxyhydroxides*, Vol. 28, 1997.
[32] S. Réguer, D. Neff, L. Bellot-Gurlet and P. Dillmann, *Deterioration of Iron Archaeological Artefacts: Micro-Raman Investigation on Cl-Containing Corrosion Products*, Vol. 38, 2007.
[33] D. Neff, P. Dillmann, L. Bellot-Gurlet and G. Beranger, *Corrosion of Iron Archaeological Artefacts in Soil: Characterisation of the Corrosion System*, Vol. 47, 2005.
[34] M. Hanesch, *Raman Spectroscopy of Iron Oxides and (Oxy)Hydroxides at Low Laser Power and Possible Applications in Environmental Magnetic Studies*, Vol. 177, 2009.

737 [35] J. Warkus and M. Raupach, *Modelling of reinforcement corrosion – geometrical effects on*
738 *macrocell corrosion*, Materials and Corrosion 61 (2009), .
739